Mesoporous ZnO@Co_3O_4 Nanosphere for Sensitive Detection of 3-Hydroxy-2-Butanone

Xinxin Tian
University of Shanghai for Science and Technology
Ming Yin
University of Shanghai for Science and Technology
Li Zhang
University of Shanghai for Science and Technology
Tianyi Qiu
Shanghai Public Health Clinical Center
Dongpo Xu
University of Shanghai for Science and Technology
Jingxuan Qiu (jxqiu@usst.edu.cn)
University of Shanghai for Science and Technology

Research Article

Keywords: Gas sensing, Mesoporous ZnO@Co3O4 nanoshpere, 3-Hydroxy-2-Butanone

Posted Date: December 13th, 2021

DOI: https://doi.org/10.21203/rs.3.rs-1152801/v1

Abstract

The mixed semiconductor metal oxides as the gas sensor can enhance the sensitivity compared with the metal oxide respectively. In this study, the mesoporous ZnO@Co_3O_4 nanosphere was prepared through the simple hydrothermal synthesis method of ZIF-L-Zn@Co, the cage construction of mesoporous ZnO@Co_3O_4 nanosphere was remained unchanged after the calcination of the ZIF-L-Zn@Co at 600℃ for 2 h in the air. The mesoporous ZnO@Co_3O_4 nanosphere was selected as the gas sensor for the detection of 3-Hydroxy-2-Butanone. Compared with the ZnO and Co_3O_4 respectively, the mesoporous ZnO@Co_3O_4 nanosphere as the gas sensor shows the high sensitivity, selectivity and stability.

1. Introduction

As a commonly food-borne pathogenic bacterial in our living environment, such as food, water and soil [1–2], *Listeria monocytogenes* (*L.monocytogenes*) can cause pregnant women, elderly or immunocompromised people with the food-borne illnesses. Up to now, flow cytometry (FC) [3–4], Polymerase chain reaction (PCR) [5–6], dynamic light scattering (DLS) [7] and enzyme-linked immunosorbent assay (ELISA) [8] have been developed to detect *L.monocytogenes*. Most of these techniques cannot realize the point-of-care testing (POCT) due to the directly detection with expensive instruments and reagents in the laboratory, and some of these methods need the expensive antibody in the experiments. Compared with these complex detection process, the volatile signature metabolite 3-hydroxy-2-butanone (3H-2B) produced from *L.monocytrogenes* can be easily detected using the gas sensing technique. However, many potentially interfering gas species from *L.monocytrogenes* metabolites can lead to wrong results in the experiments [9]. Therefore, it is a challenge to find a selective and sensitive gas sensor to detect trace 3H-2B.

Metal oxide semiconductor (MOS) with simple applicability, low fabrication cost, and hierarchical structures such as ZnO [10], WO_3 [11], SnO_2 [12], Fe_3O_4 [13], Co_3O_4 [14], In_2O_3 [15], etc., can be used as the chemical gas sensors for the detection of harmful gases. Among these gas sensing materials, each of them has the special target gas, respectively, and usually the bimetal compound oxide can shows the better performance for the gas sensing detection.

Herein, the mesoporous ZnO@Co_3O_4 nanosphere was synthesized through a two-step hydrothermal method and used as the as gas sensor for the sensitive detection of 3H-2B. Firstly, the ZIF-L-Zn@Co nanomaterial with polyhedral structure was synthesized through the simple hydrothermal method, and secondly the mesoporous ZnO@Co_3O_4 nanosphere was obtained after the calcination of the ZIF-L-Zn@Co nanopartical at 600℃ in the air. The mesoporous ZnO@Co_3O_4 nanosphere as the gas sensor shows the better selectivity and good cycling stability at lower operating temperature of 152℃ for the detection of 3H-2B.

Experimental

2.1. Chemicals

Zinc nitrate hexahydrate, cobalt nitrate hexahydrate, dimethylimidazole, anhydrous ethanol, ammonia, formaldehyde, trimethylamine, methanol, enthanol, xylene, methylbenzene and triethylamine were purchased from Sinopharm. Chemical Regents Co., Ltd. (China). All the other chemicals and reagents are of the highest grade commercially available and used as received.

2.2 Synthesis of mesoporous ZnO@Co_3O_4 nanospheres

The ZIF-L-Zn@Co nanomaterial was synthesized as follows: 2.95 g Zinc nitrate hexahydrate and 2.89 g cobalt nitrate hexahydrate were dissolved in 400 ml water forming the homogenous solution under stirring, and then 13 g dimethylimidazole and 6 mL triethylamine were added into the solution and reacted for 3 h. The finally obtained solid particles were washed 3 times with deionized water, and dried at 80℃ for 12 h. The mesoporous ZnO@Co_3O_4 nanospheres were finally obtained after the calcination of the ZIF-L-Zn@Co at 600℃ in the air with the heat rate of 2℃ min^{-1}.

2.3 Characterization

The pore size distribution and Brunauer-Emmett-Teller (BET) specific surface area of the material were determined by ASIC-2 gas adsorption analyzer (N_2 as adsorbent and operating temperature of -196 C). The scanning electron microscope (SEM) and transmission electron microscope (TEM) images of the samples were detected by Quanta FEG 450 and HT7800 to characterize the morphology and microstructure of the materials. The crystallinity of the product was analyzed by Brooke D4 X-ray diffractometer at 40 kV and 40 mA. X-ray photoelectron spectroscopy (XPS, Thermo Scientific, Escalab 250) was used for elemental analysis of the samples. The gas sensitivity of the materials was tested by semiconductor characterization system (Weisheng HW-30A, China).

2.4. Gas sensing value of samples

The manufacturing method of the sensor and the gas sensitivity test of the sensor are as follows: First, a small amount of the prepared sample was taken into uniform powder and dropped into anhydrous ethanol to form the paste, and then the paste was coated on the surface of the ceramic tube, a nickel-chromium alloy coil was inserted into the ceramic tube. Finally, the uniformly coated ceramic tube was dried at room temperature and aged at 246℃ in air for one week to improve the stability of the device. 3H-2B was detected using a semiconductor characterization system (Weisheng HW-30A, China) in a chamber with relative humidity at 50-70%. The ratio of air resistance (Ra) to target gas resistance (Rg) was selected as the gas sensing response of the sensors.

3. Results And Discussion

3.1. Synthesis and characterization of mesoporous ZnO@Co_3O_4 nanosphere and its application as gas sensor

The synthesis of mesoporous ZnO@Co_3O_4 nanosphere and its application as gas sensor are shown in Fig. 1. ZIF-L-Zn@Co was synthesized through the hydrothermal method, the mesoporous ZnO@Co_3O_4 nanosphere composed with small nanosheets was obtained after the calcination of the ZIF-L-Zn@Co at 600℃ in the air. Mesoporous ZnO@Co_3O_4 nanosphere as gas sensor shows the well performance for the detection of 3H-2B.

The morphology and size of the ZIF-L-Zn@Co and mesoporous ZnO@Co_3O_4 nanosphere were analyzed by SEM. As shown in Fig. 2a, the ZIF-L-Zn@Co nanocomposite is composed of polyhedral nanoparticals with different sizes, and after the calcination at 600℃ in the air, the mesoporous ZnO@Co_3O_4 shows the nanosphere structure composed with many metal oxides nanosheets. The TEM images in Fig. 2c and Fig. 2d show the crystal structure of the mesoporous ZnO@Co_3O_4 nanosphere, which is corresponding with the XRD results.

In order to study the crystal structure mesoporous ZnO@Co_3O_4 nanosphere, the samples were analyzed by XRD. As shown in **Fig.3**, ten diffraction peaks of (100), (002), (101), (102), (110), (103), (200), (112), (201) and (202) belong to ZnO were observed according to the standard card (PDF # 36-1451), and the diffraction peaks of (111), (220), (311), (222), (400), (422), (511), (440), (620), (533) and (622) were Co_3O_4 according to the standard card (PDF # 43-1003). No other impurity peaks were observed, indicating that the composite is composed of ZnO and Co_3O_4. According to Scherrer equation, the average particle size of ZnO@Co_3O_4 is 25.95 nm.

The surface chemical states and elemental composition of mesoporous ZnO@Co_3O_4 nanosphere were further studied by XPS technique. **Fig.4** shows the XPS spectrum of mesoporous ZnO@Co_3O_4 nanosphere with Zn, Co and O elements (**Fig. 4a)**. For Zn 2p orbitals, according to the standard XPS spectra of ZnO, Zn $2p_{3/2}$ and Zn $2P_{1/2}$ peaks appear at 1021.34 eV and 1044.41 eV (**Fig. 4b**), respectively, and the spin orbital splitting value is 23 eV, which is related to Zn^{2+} ions. As shown in **Fig. 4c**, the obvious high resolution peak is corresponding to the two main peaks of Co $2p_{3/2}$ and Co $2P_{1/2}$, and the binding energy is located at 779.50 eV and 794.60 eV, respectively. At 790 eV, it has Co^{3+} characteristics of typical oscillation structure [16]. In addition, there are two sat-ellites at 788.83 eV and 804.07 eV. Oxygen vacancy is beneficial to the work of gas sensor, and it is convenient to improve the type and content of oxygen adsorbed on the surface. Therefore, in order to explore the changes of oxygen adsorption on the surface, the energy spectrum of sample O 1s XPS was analyzed, and the results are shown in **Fig. 4d**. O 1s spectrum can be divided into three peaks: 529.20 eV (lattice oxygen), 530.70 eV (vacancy oxygen) and 531.50 eV (surface chemisorbed oxygen) [17].

The specific surface area and pore size of the sample were measured by nitrogen adsorption and desorption. As shown in **Fig. 5a**,the hysteresis characteristic is typical of type IV isotherm type H3 hysteric

ring. The hysteresis characteristic increases significantly when the relative pressure (P/P_0) is 0.8-1.0, and capillary aggregation occurs in the adsorbent, proving the existence of mesoporous structure [18]. The BET -specific surface area of $ZnO@Co_3O_4$ is 17.495 m^2/g, which is much higher than that of pure zinc oxide (9.89 m^2/g) [19], that can better improve the gas sensitive characteristics. The Barrett-Joyner-Halenda (BJH) method was used to calculate the pore distribution of the desorption, with an average pore diameter of 23.05 nm **(Fig. 5b)**

3.2. Gas sensing properties

Mesoporous $ZnO@Co_3O_4$ nanosphere are used to make gas sensors to evaluate their gas sensitive properties. Temperature is considered to be one of the key parameters that affect the response value of gas sensitive experiment. It affects the performance of gas sensor by affecting other parameters of resistance machine. In order to find the optimal operating temperature of the equipment, 30 ppm, 40 ppm and 50 ppm 3H-2B gases were selected respectively, and the gas sensitivity test was conducted at 120-250℃. The results are shown in Fig. 6a. The curves show two peak values at 152℃ and 205.14℃, and the response values are above 12. This may be due to the influence of temperature on the formation of reactive oxygen species and the adsorption of target gas molecules on the sensor surface [20]. Since the gas molecules are more stable at a lower temperature, and the experimental conditions are more suitable for low temperature, 152℃ is selected as the best working temperature in the subsequent work.

Similarly, gas selectivity is another key parameter of the sensing device in practical work detection. Under the optimum working conditions, the responses of several common volatile gases (such as 3H-2B triethylamine, trimethylamine, ammonia, formaldehyde, ethanol, isoprene, xylene and methanol) were tested. The corresponding response values at the concentration of 50 ppm are shown in **Fig. 6c.** As shown in the figure, the response value of the sensor to 3H-2B is the highest, which is 12.64, while the response value of the other gases are respectively 1.738, 1.653, 1.560, 1.524, 1.397, 1.210, 1.127, 1.065. This indicates that at 152℃, the sensor based on $ZnO@Co_3O_4$ has the strongest response to 3H-2B at 50 ppm, which is 7-12 times higher than the response of other various testing gases, showing excellent selectivity to 3H-2B. **Fig. 6b** and **Fig. 6d** show the response value and resistance image of the mesoporous $ZnO@Co_3O_4$ nanosphere circulating at 152℃, 50 ppm gas. mesoporous $ZnO@Co_3O_4$ nanosphere sensor has been cycled four times in the test chamber, and the results can be seen the sensor has good reproducibility and stability.

The response and recovery time of 3H-2B is 90% of the time that the resistance of the sensor changes during adsorption and desorption. **Fig. 7a** and **Fig. 7d** show the response and recovery curves of the mesoporous $ZnO@Co_3O_4$ nanospheresensor to 3H-2B in the concentration range of 0.5-50 ppm at 152℃. The response value increases with increasing concentration. Further explore the relationship between the sensor's response value to 3H-2B and the linearity of the concentration. The results are shown in **Fig. 7b**. At 0.5-50 ppm, there is a relatively ideal linear relationship, R^2=0.9862. At a concentration of 30 ppm, the response time of the mesoporous $ZnO@Co_3O_4$ nanosphere is 77 s and the recovery time is 20 s (**Fig. 7c**).

As shown in the **Fig. 8,** under the working condition of 152℃ and the same humidity, the maximum response value of pure ZnO sensor to 3H-2B at 50 ppm is very unstable, ranging from 36.08 to 115.40, with a large fluctuation range. The maximum response value of pure Co_3O_4 sensor under the same working conditions is 8.30 (response value =Rg /Ra). The maximum response value of the mesoporous ZnO@Co_3O_4 nanosphere sensor was stable at 12.64.

3.3 Mechanism on the mesoporous ZnO@Co_3O_4 nanosphere sensing properties

It is well known that the response of traditional sensor materials depends on their ability to absorb oxygen species on the surface, and the chemical reaction of the sensor can adjust the concentration of charge, thus reducing the resistance value corresponding to the gas sensing performance. However, it is worth mentioning that the resistance value decreases or increases depending on the type of semiconductor (including n-type and p-type) of the inductive material. ZnO@Co_3O_4 nanoparticles are n-p-type heterostructures composed of n-type and p-type materials.

According to the previous experience of gas sensitivity testing, when CoO is p-type semiconductor, the composite sensor material will show the typical conduction behavior of n-type semiconductor. As a result, the electron concentration can regulate the resistance value generated by the heterojunction sensing material. Therefore, the mechanism of gas sensing is mainly attributed to electron transfer under heterojunction structure.

The sensor reaction generally consists of two stages: oxidation and reduction of the material surface. In the reduction condition, oxygen vacancies were located on the surface of ZnO@Co_3O_4 nanocomposites. Under the oxidation condition, oxygen molecules were adsorbed on the surface of nanocomposite gradually with gas sensitive reaction. After that, oxygen molecules were converted into oxygen species by extracting free electrons from the conduction of the heterojunction sensing material, and the formula is as follows:

$O_2(gas) \rightarrow O_2(ads)$ (1)

$O_2(ads) + e^- \rightarrow O_2^-(ads)$ (T＜100°C) (2)

$O_2^-(ads) + e^- \rightarrow 2O^-(ads)$（100°C＜T＜300°C） (3)

$O^-(ads) + e^- \rightarrow O^{2-}(ads)$（T＞300°C） (4)

Electrons in the material are depleted by oxygen adsorption, forming an electron depletion layer during the process. When reductive 3H-2B is injected into the chamber with a microsyringe, redox reactions occur in a negative oxygen environment and electrons are again released into the conduction band. When the thickness of the electron depletion layer decreases with the reaction, oxygen vacancies are re-formed.

When the material is again exposed to air, the oxygen vacancies recombine and the ZnO@Co_3O_4 sensor returns to a high resistance state.

$C_4H_8O_2 + 10\ O^-(ads) \rightarrow 4\ CO_2 + 4\ H_2O + 10e^-$ (5)

$C_4H_8O_2 + 10\ O^{2-}(ads) \rightarrow 4\ CO_2 + 4\ H_2O + 20e^-$ (6)

4. Conclusion

In summary, the mesoporous ZnO@Co_3O_4 nanosphere was obtained after the calcination of ZIF-L-Zn@Co, which was synthesized through a simple hydrothermal method. The mesoporous ZnO@Co_3O_4 nanosphere was selected as the gas sensor for the detection of 3H-2B. Compared with the ZnO and Co_3O_4 respectively, the mesoporous ZnO@Co_3O_4 nanosphere shows the high sensitivity, selectivity and stability. Through the detection of 3H-2B, the mesoporous ZnO@Co_3O_4 nanosphere can be used for the indirect detection of *Listeria Monocytogens* in the real samples.

Declarations

Declaration of Competing Interest

There are no conflicts of interest to declare.

Acknowledgments

This work was supported by the National Natural Science Foundation of China (32000470).

References

1. D. Luo, X. Huang, Y. Mao, C. Chen, F. Li, H. Xu, Y. Xiong, Two-step large-volume magnetic separation combined with PCR assay for sensitive detection of Listeria monocytogenes in pasteurized milk. J. Dairy Sci. 2017, 100 (10), 7883-7890
2. L. Aude, S. Aymé, J. Claudy, P. Pascal, H. Alain, Biotic and abiotic soil properties influence survival of Listeria monocytogenes in soil. Plos One **8**(10), e75969 (2013)
3. F. Li, F. Li, Z.P. Aguilar, Y. Xiong, H. Xu, Polyamidoamine (PAMAM) dendrimer-mediated biotin amplified immunomagnetic separation method coupled with flow cytometry for viable Listeria monocytogenes detection. Sens. Actuators B **257**, 286–294 (2018)
4. X. Meng, G. Yang, F. Li, T. Liang, W. Lai, H. Xu, Sensitive Detection of Staphylococcus aureus with Vancomycin-Conjugated Magnetic Beads as Enrichment Carriers Combined with Flow Cytometry. ACS Applied Materials & Interfaces 2017, 9 (25), 21464–21472
5. Y. Mao, X. Huang, S. Xiong, H. Xu, Z.P. Aguilar, Y. Xiong, Large-volume immunomagnetic separation combined with multiplex PCR assay for simultaneous detection of Listeria monocytogenes and

Listeria ivanovii in lettuce. Food Control **59**, 601–608 (2016)

6. X. Meng, F. Li, F. Li, Y. Xiong, H. Xu, Vancomycin modified PEGylated-magnetic nanoparticles combined with PCR for efficient enrichment and detection of Listeria monocytogenes. Sens. Actuators B **247**, 546–555 (2017)
7. X. Huang, Z. Xu, Y. Mao, Y. Ji, H. Xu, Y. Xiong, Y. Li, Gold nanoparticle-based dynamic light scattering immunoassay for ultrasensitive detection of Listeria monocytogenes in lettuces. Biosens. Bioelectron. **66**, 184–190 (2015)
8. R. Chen, X. Huang, H. Xu, Y. Xiong, Y. Li, Plasmonic Enzyme-Linked Immunosorbent Assay Using Nanospherical Brushes as a Catalase Container for Colorimetric Detection of Ultralow Concentrations of Listeria monocytogenes. ACS Appl. Mater. Interfaces. **7**(51), 28632–28639 (2015)
9. Y. Zhu, Y. Zhao, J. Ma, X. Cheng, J. Xie, P. Xu, H. Liu, H. Liu, H. Zhang, M. Wu, A.A. Elzatahry, A. Alghamdi, Y. Deng, D. Zhao, Mesoporous Tungsten Oxides with Crystalline Framework for Highly Sensitive and Selective Detection of Foodborne Pathogens. J. Am. Chem. Soc. **139**(30), 10365–10373 (2017)
10. X. Zhou, Y.H. Zhu, W. Luo, Y. Ren, P.C. Xu, A.A. Elzatahry, X.W. Cheng, A. Alghamdi, Y.H. Deng, D.Y. Zhao, Chelation-assisted soft-template synthesis of ordered mesoporous zinc oxides for low concentration gas sensing, J. Mater. Chem. A, 2016, (4), 15064–15071
11. C.B. Zhai, M.M. Zhu, L. Jiang, T.Y. Yang, Q. Zhao, Y. Luo, M.Z. Zhang, Fast triethylamine gas sensing response properties of nanosheets assembled WO3 hollow microspheres. Appl. Surf. Sci. **463**, 1078–1084 (2019)
12. T. Zhai, H. Xu, W. Li, H. Yu, Z. Chen, J. Wang et al., Low-temperature in-situ growth of SnO2 nanosheets and its high triethylamine sensing response by constructing Au-loaded ZnO/SnO_2 heterostructure. J. Alloy. Compd. **737**, 603–612 (2018)
13. X. Song, Q. Xu, T. Zhang, B. Song, C. Li, B. Cao, Room-temperature, high selectivity and low-ppm-level triethylamine sensor assembled with Au decahedrons-decorated porous α-Fe_2O_3 nanorods directly grown on flat substrate. Sens. Actuators B **268**, 170–181 (2018)
14. Y. Xu, T. Ma, L. Zheng, L. Sun, X. Liu, Y. Zhao et al., Rational design of Au/Co_3O_4-functionalized $W_{18}O_{49}$ hollow heterostructures with high sensitivity and ultralow limit for triethylamine detection. Sens. Actuators B **284**, 202–212 (2019)
15. T.T.D. Nguyen, H.N. Choi, M.J. Ahemad, D.V. Dao, I.H. Lee, Y.T. Yu, Hydrothermal synthesis of In_2O_3 nanocubes for highly responsive and selective ethanol gas sensing. J. Alloys Compd. **820**, 153133 (2020)
16. P.H.T. Ngamou, K. Kohse-Hoeinghaus, N. Bahlawane, CO and ethanol oxidation over $LaCoO_3$ planar model catalysts: effect of the thickness, Catal. Commun. 2011, (12), 1344–1350
17. T.P. Mokoena, Z.P. Tshabalala, K.T. Hillie, H.C. Swart, D.E. Motaung, The blue luminescence of p-type NiO nanostructured material induced by defects: H_2S gas sensing characteristics at a relatively low operating temperature. Appl. Surf. Sci. **525**, 146002 (2020)

18. Y. Lü, W. Zhan, Y. He, Y. Wang, X. Kong, Q. Kuang, MOF-Templated Synthesis of Porous Co_3O_4 Concave Nanocubes with High Specific Surface Area and Their Gas Sensing Properties. ACS Appl. Mater. Inter. **6**, 4186–4195 (2014)
19. Y. Fan, Y. Xu, Y. Wang, Y. Sun, Fabrication and characterization of Co-doped ZnO nanodiscs for selective TEA sensor applications with high response, high selectivity and ppb-level detection limit. J. Alloy. Compd. **876**, 160170 (2021)
20. Y. Xu, X. Tian, P. Liu, Y. Sun, G. Du, In_2O_3 nanoplates with different crystallinity and porosity: Controllable synthesis and gas-sensing properties investigation. J. Alloy. Compd. **787**, 1063–1073 (2019)

Figures

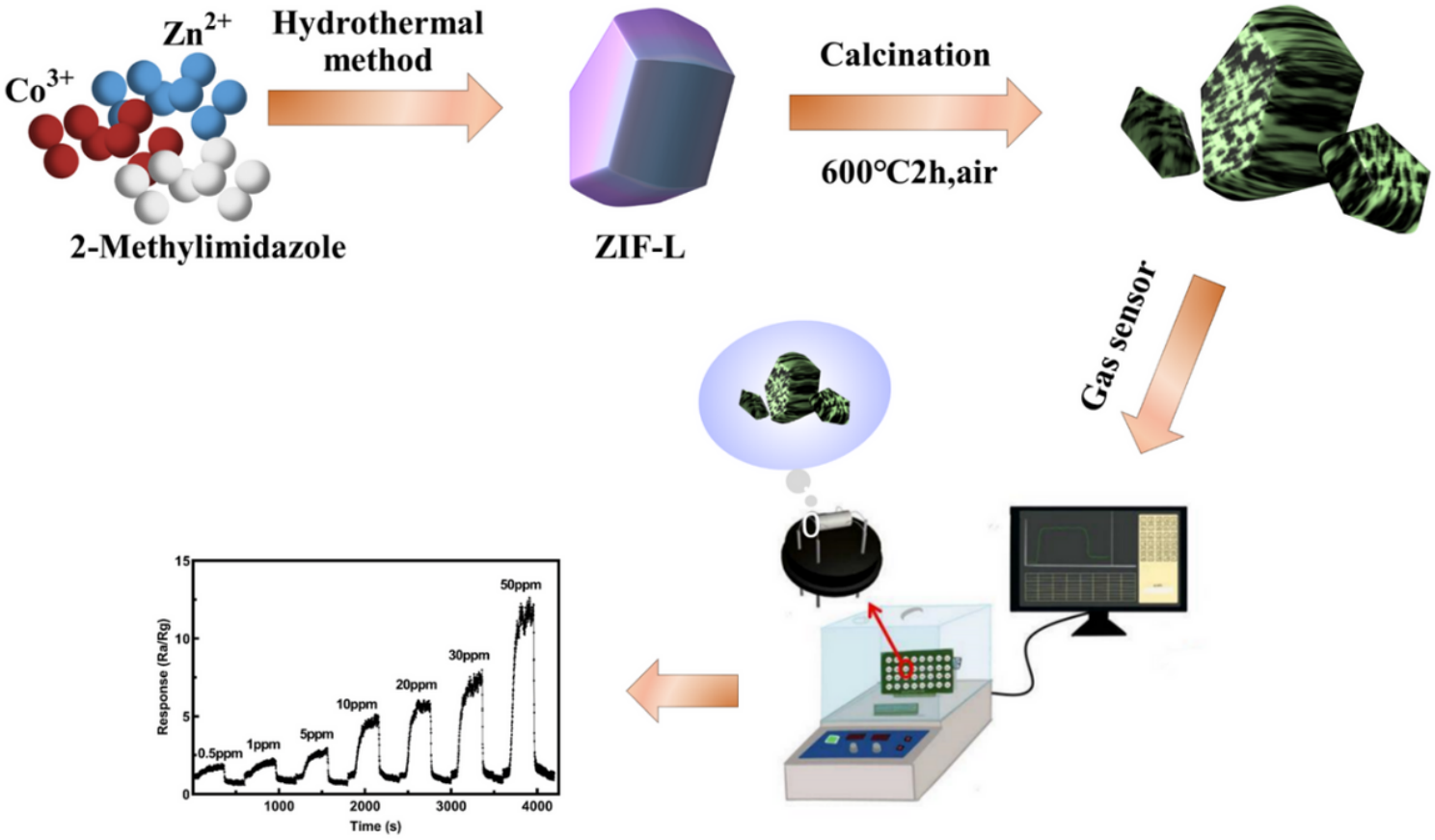

Figure 1

The synthesis schematic and application of mesoporous ZnO@Co3O4 nanosphere as gas sensor.

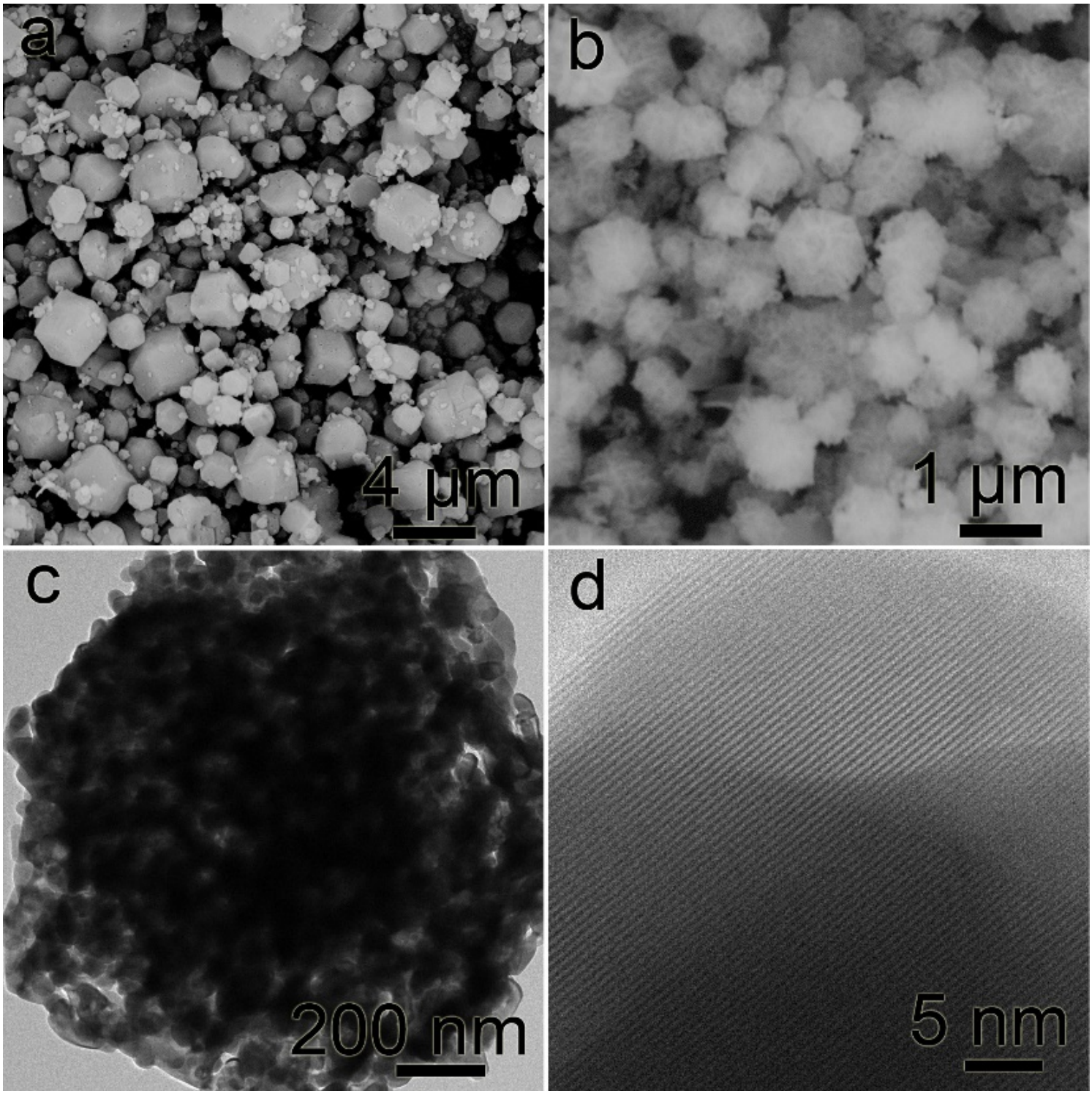

Figure 2

The SEM images of the ZIF-L-Zn@Co (a) and mesoporous ZnO@Co3O4 nanosphere (b); The TEM images of mesoporous ZnO@Co3O4 nanosphere (c, d).

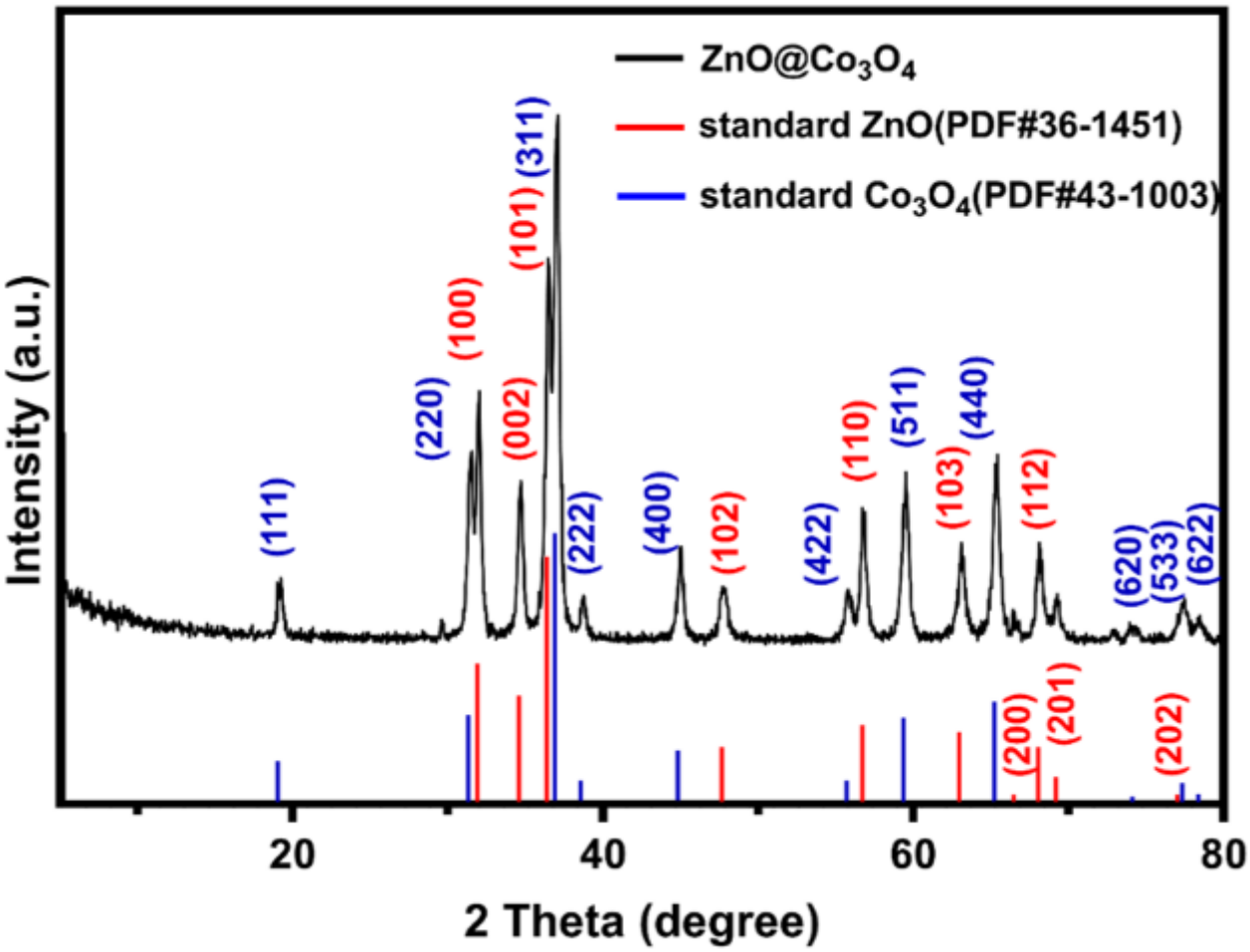

Figure 3

XRD patterns of mesoporous ZnO@Co3O4 nanosphere.

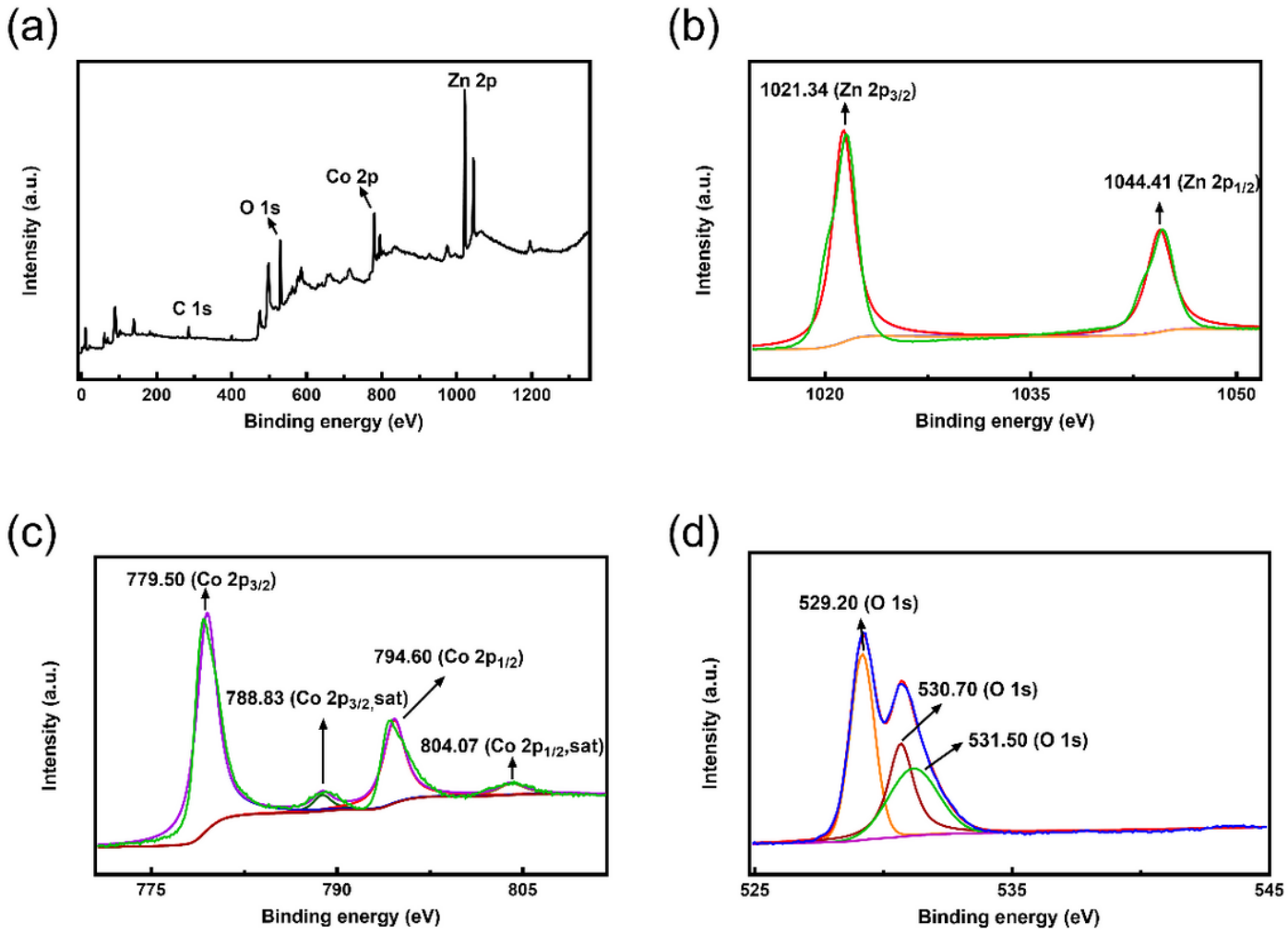

Figure 4

The XPS of mesoporous ZnO@Co3O4 nanosphere. Survey spectra (a), high-resolution XPS for Zn 2p (b), Co 2p (c) and O 1s (d).

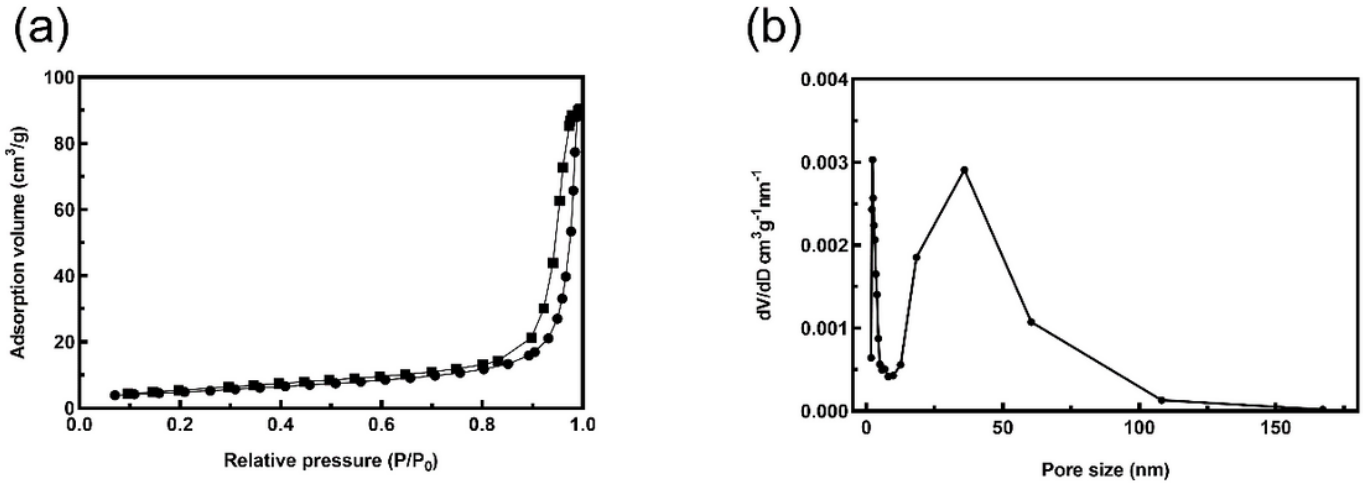

Figure 5

(a) N2 isotherm and (b) pore size distribution of mesoporous ZnO@Co3O4 nanosphere.

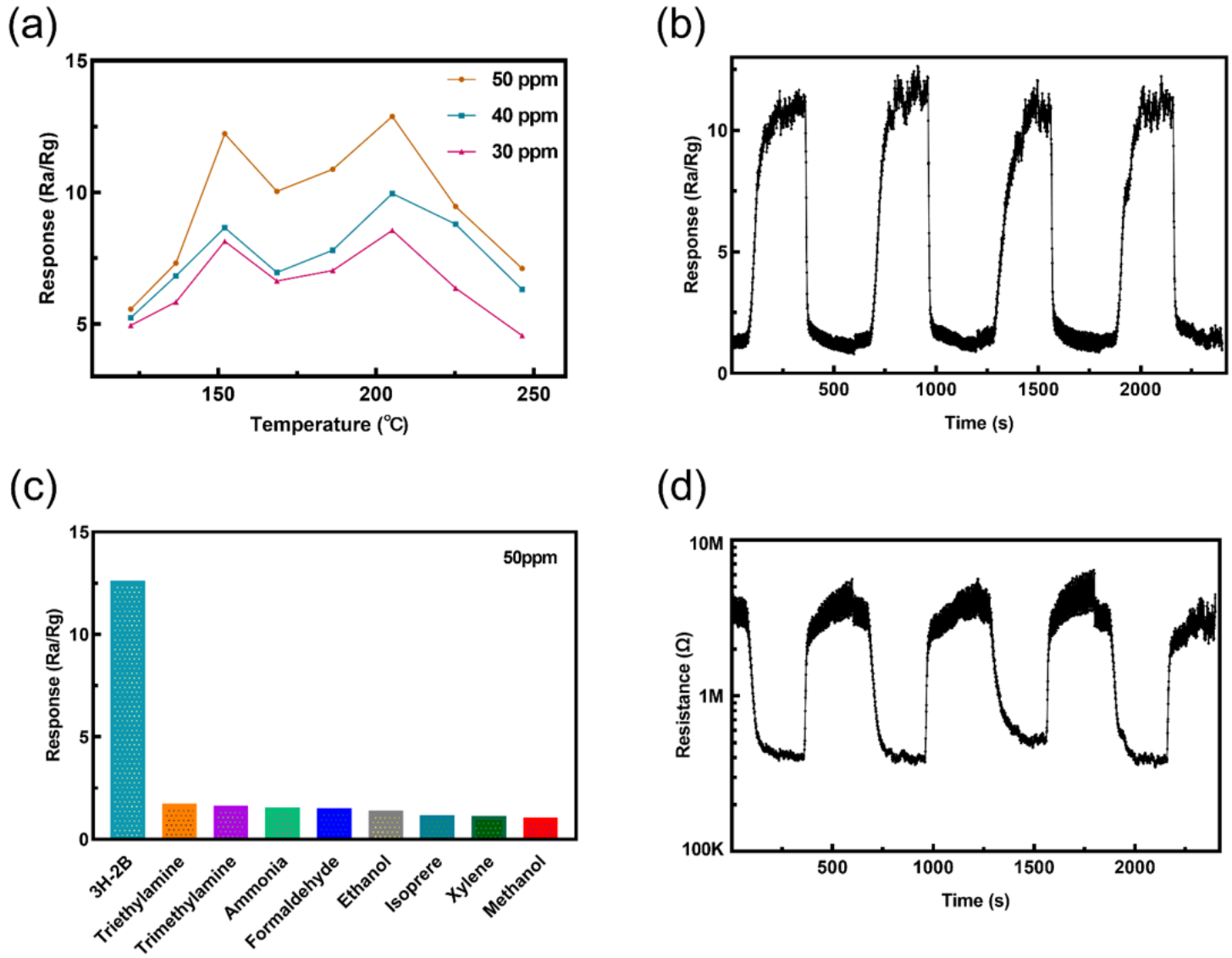

Figure 6

(a) The response of mesoporous ZnO@Co3O4 nanosphere toward 30 ppm, 40 ppm and 50 ppm 3H-2B at different control temperatures. (b) The reproducibility response toward 3H-2B at 50 ppm at 152°C. (c) The selectivity response toward different gases at 50 ppm. (d) The reproducibility of resistance toward 50 ppm 3H-2B at 152°C.

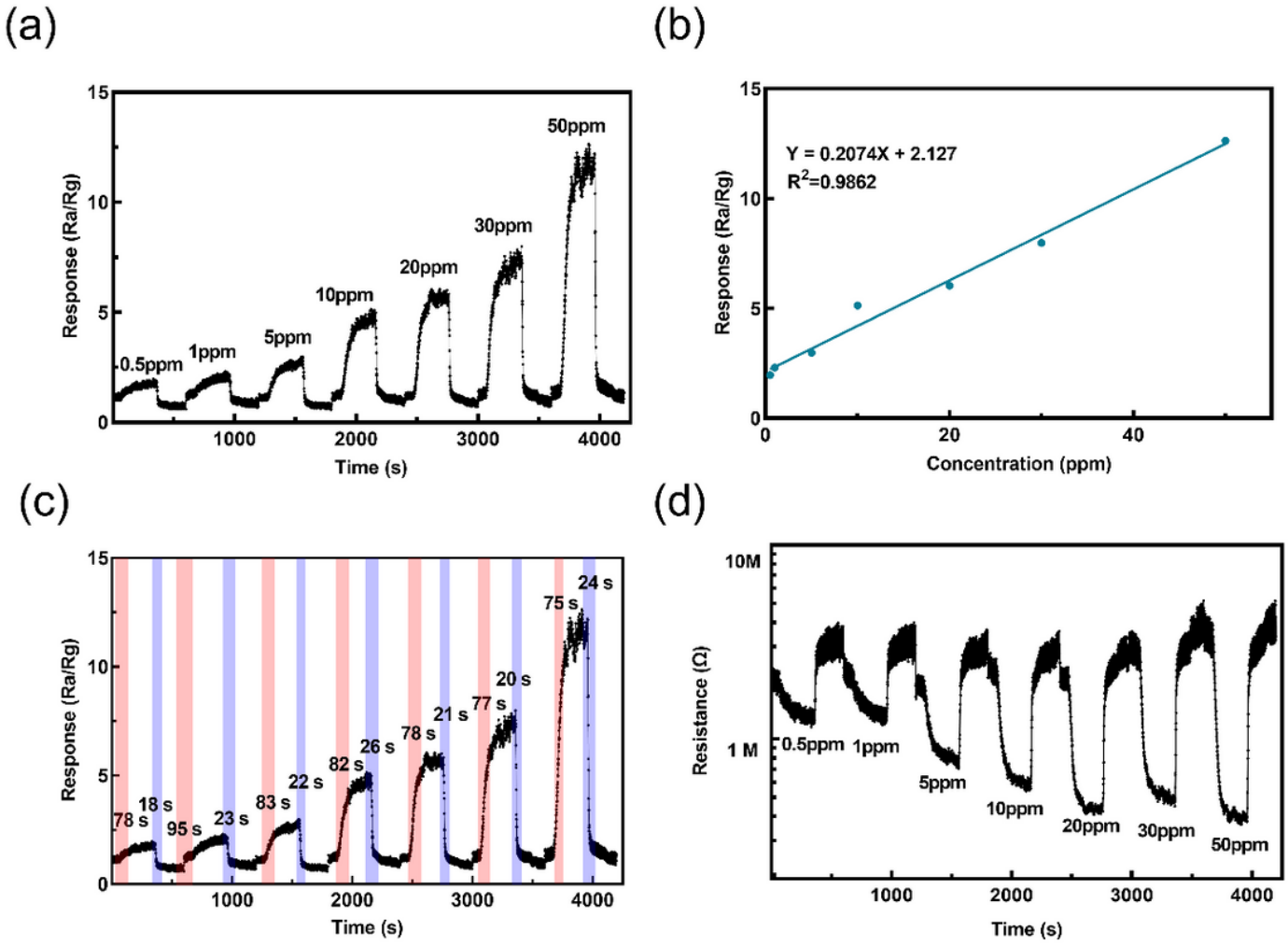

Figure 7

(a) The response toward 3H-2B at different concentrations of 0.5-50 ppm was measured at 152℃. (b) the linear response of mesoporous ZnO@Co3O4 nanosphere toward different concentrations (0.5-50 ppm) of 3H-2B measured at 152℃. (c) response and recovery curves of mesoporous ZnO@Co3O4 nanosphere toward different concentrations of 3H-2B (0.5-50 ppm) measured at 152℃. (d) the 3H-2B resistance at different concentrations (0.5-50 ppm) measured at 152℃.

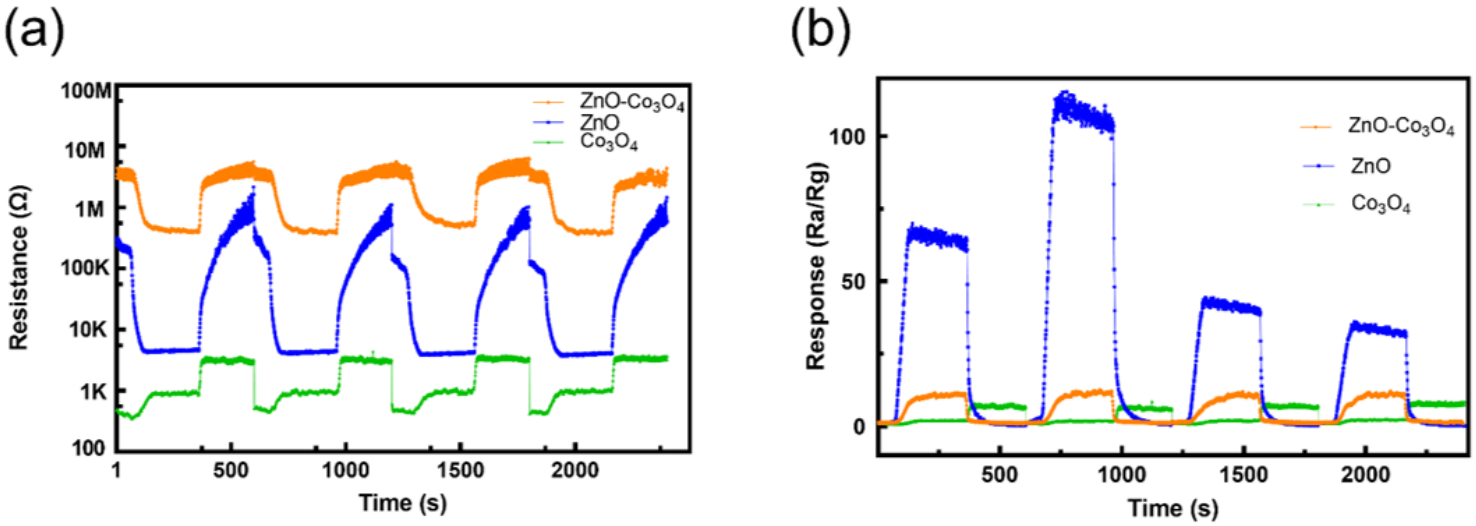

Figure 8

(a) The comparison of resistance reproducibility of the mesoporous ZnO@Co3O4 nanosphere, pure ZnO and Co3O4 at 152°C for 50 ppm 3H-2B. (b) The comparison of response reproducibility of the mesoporous ZnO@Co3O4 nanosphere, pure ZnO and Co3O4 at 152°C for 50 ppm 3H-2B.